UV Photolysis of alpha-Cyclohexanedione in the Gas Phase

ARTICLE *in* THE JOURNAL OF PHYSICAL CHEMISTRY A · MAY 2011

Impact Factor: 2.69

4 AUTHORS:

Anamika Mukhopadhyay

Indian Institute of Science Education & Rese…

19 PUBLICATIONS **63** CITATIONS

SEE PROFILE

Moitrayee Mukherjee

Indian Association for the Cultivation of Scie…

18 PUBLICATIONS **61** CITATIONS

SEE PROFILE

Arup Ghosh

University of Texas at Arlington

6 PUBLICATIONS **24** CITATIONS

SEE PROFILE

Tapas Chakraborty

Indian Association for the Cultivation of Scie…

107 PUBLICATIONS **853** CITATIONS

SEE PROFILE

THE JOURNAL OF PHYSICAL CHEMISTRY A

ARTICLE

pubs.acs.org/JPCA

UV Photolysis of α-Cyclohexanedione in the Gas Phase

Anamika Mukhopadhyay, Moitrayee Mukherjee, Arup Kumar Ghosh, and Tapas Chakraborty*

Department of Physical Chemistry, Indian Association for the Cultivation of Science, Jadavpur, Calcutta 700032, India

Supporting Information

ABSTRACT: Ultraviolet absorption spectrum of α-cyclohexanedione (α-CHD) vapor in the wavelength range of 220−320 nm has been recorded in a 1 m long path gas cell at room temperature. With the aid of theoretical calculation, the band has been assigned to the $S_2 \leftarrow S_0$ transition of largely $\pi\pi^*$ type. The absorption cross section at the band maximum (∼258 nm) is nearly 3 orders of magnitude larger compared to that for the $S_2 \leftarrow S_0$ transition of a linear α-diketo prototype, 2,3-pentanedione. The photolysis was performed by exciting the sample vapor near this band maximum, using the 253.7 nm line of a mercury vapor lamp, and the products were analyzed by mass spectrometry as well as by infrared spectroscopy. The identified products are cyclopentanone, carbon monoxide, ketene, ethylene, and 4-pentenal. Geometry optimization at the CIS/6-311++G** level predicts that the carbonyl group is pyramidally distorted in the excited S_1 and S_2 states, but the α-CHD ring does not show dissociative character. Potential energy curves with respect to a ring rupture coordinate (C−C bond between two carbonyl groups) for S_0, S_1, S_2, T_1, T_2, and T_3 states have been generated by partially optimizing the ground state geometry at DFT/B3LYP/6-311++G** level and calculating the vertical transition energies to the excited states by TDDFT method. Our analysis reveals that the reactions can take place at higher vibrational levels of S_0 as well as T_1 states.

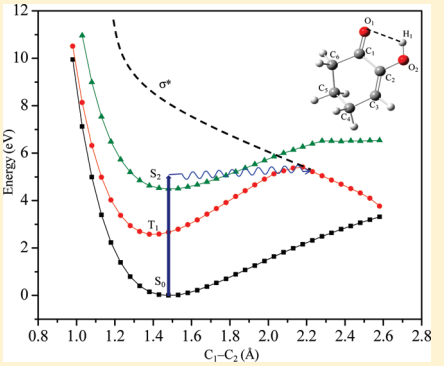

1. INTRODUCTION

Decomposition of small carbonyl compounds following near-ultraviolet (UV) excitations under gaseous condition is one of the thoroughly studied photochemical reactions.[1−15] In recent years, photodissociation studies with volatile carbonyl compounds have got renewed impetus because of implications of such photochemical reactions in atmospheric processes.[6,16−25] Typically, the reactions are initiated via cleavage of a C−C bond α to the carbonyl group following $n\pi^*$ excitation of the molecules (Norrish type I reaction).[8−13,26] The $n\pi^*$ electronic transition is symmetry forbidden and turns out to be allowed partially by means of vibronic coupling mechanism, and the corresponding band in the vapor absorption spectra typically appears as weak and structure less feature at room temperature in the wavelength range of 340−240 nm. This spectral behavior is quite general for monoketones of both cyclic and acyclic varieties.

On the other hand, the electronic absorption spectra of α-diketones display very different spectral features as diketones can belong to cyclic or acyclic categories. The two adjacent carbonyl groups in the preferred conformation of the latter category are oriented antiparallel to each other, and the longest wavelength band ($n\pi^*$ transition) practically appears in the visible range of the spectrum.[27,28] On the other hand, the cyclic α-diketones (five- and six-membered) preferentially exist in monoenol tautomeric form and gain stability by means of intramolecular hydrogen bonding.[29,30] In consequence, the electronic absorption spectral features of the latter are expected to be different from those of the former category, and as we show below that this difference influence their photodecomposition pathways. Several studies on photolysis of the linear α-diketones have been reported where biacetyl was used as prototypical system.[6,22,27] However, to our knowledge, we report here for the first time the UV absorption spectrum and photolysis of a six-membered cyclic α-diketone in the gas phase.

The prototypical structural unit of α-CHD has been found in numerous natural products,[31−33] and its 3-methyl substituted derivative is known to be responsible for aroma of coffee.[34] Recently, by measuring infrared spectra we have shown that in the gas phase the molecule exists primarily in the monoenol tautomeric form and the same tautomeric state was found almost exclusively in a cold inert gas matrix environment.[29] The compound has also been investigated using several other spectroscopic and analytical methods in the gas phase, like electronic energy loss spectroscopy,[35] ion cyclotron resonance mass spectrometry,[36] and electron diffraction spectroscopy.[37] Electronic structure calculations at different levels of theory were employed at times for theoretical prediction of the stability of its tautomers and other properties.[29] In the present paper, we report our studies on UV absorption spectral and UV-induced photolysis of the compound in the gas phase.

Received: February 2, 2011
Revised: May 27, 2011
Published: May 31, 2011

2. METHODS

UV absorption spectrum of α-CHD vapor was recorded in a home-built gas cell of path length 1 m. Light from a Xe arc lamp (Oriel) was dispersed by a 1 m monochromator (Spex, 1000M) and the selected wavelengths were passed through the gas absorption cell after collimation by a telescopic lens system. The telescope helps to maintain a uniform beam shape all through the cell length. Light intensity after traversing through the gas cell is measured with (I) and without (I_0) the sample vapor by a photomultiplier tube (PMT). The output signal of PMT, as a function of wavelength of light selected by the monochromator, is acquired into a personal computer by use of a home-built data acquisition system. The spectrum is displayed by plotting $\log(I_0/I)$ against wavelength (nm) of light.

To perform the gas phase photolysis reactions, a quartz tube of length 30 cm and inner diameter 30 mm was used as the reaction cell. The photolyzed products were analyzed by mass spectrometry as well as infrared spectroscopy. For mass spectrometric analysis the photolyzed gas mixture was introduced into the vacuum chamber of the mass spectrometer through an effusive nozzle. The molecules were ionized by an axial molecular beam ionizer and the produced ions were analyzed by a quadrupole mass analyzer. The kinetic energy of the ionizing electrons was kept very low (~11 eV) to reduce fragmentation of the parent molecular ion. The positive ions in the mass spectrometer were detected by a channel electron multiplier detector. All the mass spectrometer components were procured from Extrel CMS.

For the purpose of infrared spectral analysis of the photoproducts, the sample vapor was taken in a multipass absorption gas cell (Bruker) of effective path length 8.0 m. The IR spectra were recorded before and after irradiation of α-CHD vapor using an FTIR spectrometer model (model IFS 66s Bruker optics). All spectra were recorded using an instrumental resolution of 1.0 cm^{-1}.

Quantum chemistry calculation has been performed for theoretical predictions of the ground and excited state geometries of α-CHD and its fragments by use of Gaussian 03 program package.[38]

3. RESULTS AND DISCUSSION

3.1. Excited States of α-CHD: UV Absorption Spectrum. Figure 1 shows the UV absorption spectrum of α-CHD vapor. The vapor pressure of the sample in the gas absorption cell (1 m path length) was 0.01 mbar at 22 °C temperature. The spectrum, within the displayed spectral range, is manifested as a structureless band whose maximum appears at 258 nm, and the absorption tail in longer wavelength is extended up to 280 nm. We have noted that the band shape is not altered upon mixing of dry argon at different partial pressures with the sample vapor in the absorption cell, and this eliminates the possibility for formation of any intermolecular association complex under the condition of measurements. The absorption cross-section (base e) at different wavelengths across the band profile is estimated using the relation, $A = \sigma lN$ and shown using small squares (red) with error bars. Here, A denotes absorbance, σ is absorption cross section, l is the path length of the gas cell used, and N is the density of absorbing molecule, i.e., number of molecules per unit volume. N is estimated using the relation, $N = PN_A/RT$, where N_A is the Avogadro number.

The electronic absorption spectrum of the compound in methylcyclohexane solution at room temperature is shown in the inset (Figure 1). The band shape appears similar to that of the vapor absorption spectrum except a few nanometers shifting of the band maximum to longer wavelengths. This indicates that the electronic transitions responsible for the observed band are not perturbed significantly upon dissolving the compound in hydrocarbon solution.

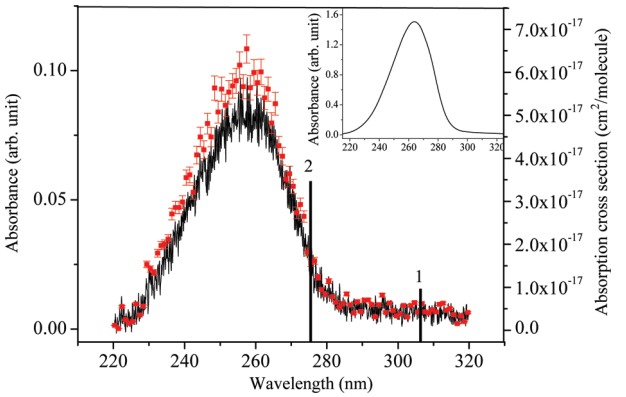

Figure 1. UV absorption spectrum of α-CHD vapor at room temperature (black curve). The absorption cross sections (base e) estimated at different wavelengths are shown using red squares. The wavelengths predicted for vertical excitations to the two lowest electronic energy levels ($S_1 \leftarrow S_0$ and $S_2 \leftarrow S_0$), calculated by TDDFT/B3LYP/6-311++G** method, are denoted by two vertical lines. The inset shows the UV absorption spectrum of α-CHD in methylcyclohexane solution at room temperature.

For an idea about the nature of the electronic transition responsible for this band, and also to correlate the spectral features with the molecular structure, we present here a brief comparative discussion of the spectrum of α-CHD with those of five analogous molecules shown in Table 1. Some striking contrasts are the following. First, the λ_{max} for the first electronic absorption bands ($S_1 \leftarrow S_0$) of all the five molecules appear at wavelengths longer compared to that of the only band of α-CHD (Figure 1). Most notably, the λ_{max} of the present system appears at a shorter wavelength compared to those of the monoketones, linear (acetone) as well as cyclic (cyclohexanone). Second, it has been also noted that the absorption tails of the two monoketone bands are extended to much longer wavelengths compared to that of present system. Apparently, such spectral behavior of α-CHD must be uncharacteristic, because, in the enol tautomeric form of α-CHD the carbonyl group is in electronic conjugation with the ethylene group and also the enolic group of the molecule is intramolecularly hydrogen bonded with the carbonyl group in the gas phase. The effect of conjugation between C═O and C═C groups within the same molecule on the λ_{max} values is manifested in the spectra of methylvinylketone (MVK) and cyclohexenone. As expected, the λ_{max} values in $S_1 \leftarrow S_0$ spectra of the two molecules appear at much longer wavelengths, 325 and 320 nm, respectively, compared to those of acetone and cyclohexanone. In striking contrast, although α-CHD has the same structural motif, the λ_{max} appears at a much shorter wavelength (258 nm). Finally, the contrasts with respect to the band positions of the biacetyl are even more drastic.[27] The λ_{max} of a band assigned to $S_2 \leftarrow S_0$ transition of biacetyl (273 nm) appears at a longer wavelength than the λ_{max} (258 nm) of the only band observed for the present system. In conclusion, considering all such contrasts, it appears that the observed band in Figure 1 is arising primarily due to $S_2 \leftarrow S_0$ transition and the

Table 1. Absorption Maxima (λ_{max}) in the Measured $S_1 \leftarrow S_0$ and $S_2 \leftarrow S_0$ Electronic Absorption Spectra of Selected Mono- and Diketones Shown along with the Calculated (TDDFT/6-311++G) Wavelengths for Vertical Excitations to the Two Electronic States[a]**

Molecule	$S_1 \leftarrow S_0$			$S_2 \leftarrow S_0$		
	λ_{max} (nm) Measured	λ_{vert} (nm) Calculated	assignment	λ_{max} (nm) Measured	λ_{vert} (nm) Calculated	assignment
Cyclohexanone	290 [a]	295	$n\rightarrow\pi^*$ [a]	195 [a]	213	$n\rightarrow\sigma^*_{CO}$ [a]
Cyclohexenone	320 [b]	345	$n\rightarrow\pi^*$	218	219 [b]	$\pi\rightarrow\pi^*$
Acetone	280 [d]	281	$n\rightarrow\pi^*$ [d]	194 [c]	213	$n\rightarrow 3s$ [c]
MVK	325 [f]	355	$n\rightarrow\pi^*$	195 [e]	216	$\pi\rightarrow\pi^*$
Biacetyl	425 [g]	460	$n\rightarrow\pi^*$	273 [g]	274	$n\rightarrow\pi^*$
α-CHD	–	307	$n\rightarrow\pi^*$	258	275	$\pi\rightarrow\pi^*$

[a] The assignments are suggested by visualizing the molecular orbitals involved in the respective transitions. [b] Reference 42. [c] NIST Database. [d] Reference 9. [e] Reference 12. [f] Reference 15. [g] Reference 25. [h] Reference 27.

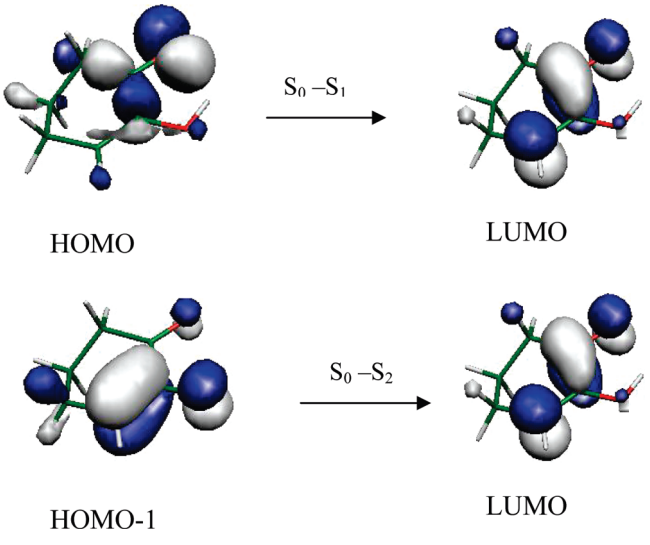

Figure 2. Molecular orbitals of α-CHD associated with $S_1 \leftarrow S_0$ and $S_2 \leftarrow S_0$ electronic transitions. For both transitions, electronic excitation takes place to a common antibonding orbital (LUMO) from HOMO and HOMO-1 orbitals.

first transition ($S_1 \leftarrow S_0$) is somehow much strictly forbidden and does not show up in the spectrum. This conclusion is consistent with the theoretical predictions as mentioned in the following paragraph.

The predicted (TDDFT/B3LYP/6-311++G**) vertical transition wavelengths to the two electronic states of α-CHD are indicated by two vertical lines in Figure 1, and those of the other five molecules are presented in Table 1. The nature of molecular orbitals involved ($n\pi^*$, $\pi\pi^*$, etc.) in the two electronic transitions of all the molecules have been found out by visualizing the orbitals using Molekel software package. Thus, the correspondences between the measured λ_{max} and calculated vertical transition wavelengths for $S_1 \leftarrow S_0$ and $S_2 \leftarrow S_0$ transitions of those five molecules appear to be very good, and this provides a confidence that the predictions of the calculation performed here are quite realistic. Now for the present system, the same level of calculation predicts that the vertical transition wavelength for $S_2 \leftarrow S_0$ transition is 275 nm, which is quite consistent with the observed λ_{max}. Furthermore, intensity for this transition is predicted to be nearly 300 times larger compared to that for $S_1 \leftarrow S_0$ transition. The predicted wavelength for the latter is 307 nm, and it is similar to those of cyclohexenone and MVK, but absence of any band in the measured spectrum indicates that the transition is forbidden.

In Figure 2, we have shown the pictures of the molecular orbitals (MOs) associated with $S_1 \leftarrow S_0$ and $S_2 \leftarrow S_0$ transitions predicted by TDDFT calculation. These two transitions correspond to electron promotion from the HOMO to LUMO and HOMO−1 to LUMO, respectively. The orbital diagram indicates that electronic excitation to S_1 is $n\pi^*$ type but S_2 has significant extent of $\pi\pi^*$ character. Further discussions on

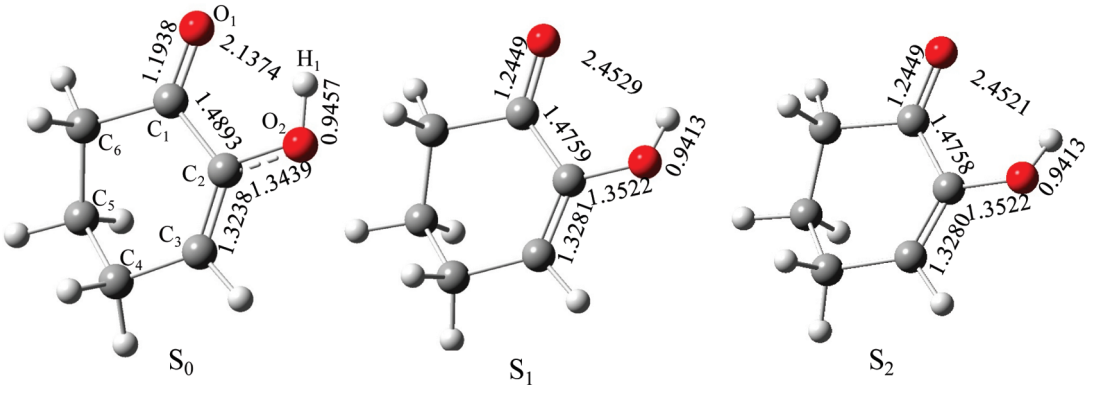

Figure 3. Optimized structures of α-CHD in S_0, S_1, and S_2 states calculated by HF/6-311++G** and CIS/6-311++G** methods for the ground and excited states, respectively. A few bonds are labeled with the optimized values of bond lengths. The details are presented in Table 2.

Table 2. Selected Geometric Parameters Corresponding to the Optimized Structures of α-CHD in the Ground (S_0) and Two Lowest Excited Singlet Electronic States (S_1 and S_2)[a]

parameters	S_2	S_1	S_0 (our work)[b]	Shen's work[c]
C_1-O_1 (Å)	1.2449	1.2449	1.1938	1.1928
C_1-C_2 (Å)	1.4758	1.4759	1.4893	1.4899
C_2-O_2 (Å)	1.3522	1.3522	1.3439	1.3437
C_2-C_3 (Å)	1.3280	1.3281	1.3238	1.3232
O_2-H_1 (Å)	0.9413	0.9413	0.9457	0.9456
O_1-H_1 (HB distance) (Å)	2.4521	2.4529	2.1374	
$\angle C_1-C_2-O_2$ (deg)	116.84	116.84	115.39	115.06
$\angle C_2-O_2-H_1$ (deg)	111.09	111.08	108.52	
$\angle O_1-C_1-C_2$ (deg)	121.92	121.91	119.35	119.26
$\tau_1(O_1-C_1-C_2-O_2)$ (deg)	−14.06	−14.06	1.83	
$\tau_2(C_1-C_2-O_2-H_1)$ (deg)	−28.12	−28.26	−0.73	
$\tau_3(O_1-C_1-C_2-C_6)$ (deg)	158.70	158.68	177.68	
$\tau_4(O_1-C_1-C_6-C_5)$ (deg)	168.26	168.27	151.15	

[a] Some of the ground state geometric parameters of the molecule reported in ref 37 are reproduced here for comparison. [b] Calculated at the HF/6-311++G** level. [c] HF/6-311G** level, ref 37.

photochemical implications of these electronic excitations are presented in the following section.

3.2. Excited States of α-CHD: Geometry in the Low-Lying Excited States. Fully optimized structures of the stable enol tautomeric form of the molecule in the ground and two lowest excited singlet states (S_1 and S_2) are shown in Figure 3, and some pertinent geometrical parameters for these states are presented in Table 2. The molecular geometry in the ground electronic state of α-CHD was optimized at HF/6-311++G** and DFT/B3LYP/6-311++G** levels, and that for the two excited singlet states were optimized at CIS level using the same basis set. The carbonyl group in the two excited states appears considerably distorted in comparison to the ground state. The C═O bond length is increased by ∼0.05 Å, and the values of the four dihedral angles, τ_1, τ_2, τ_3, and τ_4 (Table 2), are also largely altered. The nature of the changes indicates pyramidal distortion of the carbonyl group in the excited states. As a consequence, the intramolecular OH···O hydrogen bond is weakened and the hydrogen bond distance turns out to be longer by ∼0.3 Å. The other interesting prediction is shortening of the C_1-C_2 bond length in the optimized geometry in the two electronic states and it is consistent also with displayed orbital picture of LUMO in Figure 2, where a π-bond is formed between the C_1 and C_2 atoms and that results in shortening of this bond length. This also implies that the C_1-C_2 bond breaking is not favorable in the excited state prepared by direct light excitation. An NBO analysis performed at the B3LYP/6-311++G** level on the optimized geometries of the three electronic states reveals that the n(O) → σ^*(O−H) hyperconjugation energy of the intramolecular OH···O hydrogen bond in the S_0, S_1, and S_2 electronic states are 3.72, 0.5, and 0.51 kcal/mol, respectively. Obviously, the reduction in hyperconjugation energy in the excited states is the consequence of geometry distortion, which results in weakening of the hydrogen bonds.

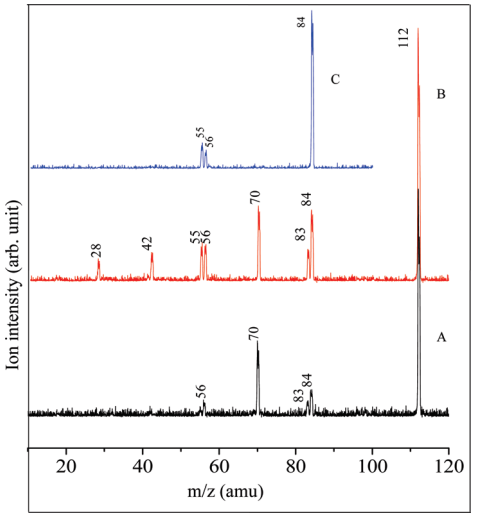

Figure 4. Electron ionization mass spectra of α-CHD (A) before and (B) after UV exposure of the sample vapor. Kinetic energy of ionizing electrons was kept low, 11 eV, to reduce fragmentation. (C) Mass spectrum of pure cyclopentanone vapor recorded under the same mass spectrometric condition.

4. ANALYSIS OF PHOTOPRODUCTS

4.1. Quadrupole Mass Spectrometry. The mass spectra of the α-CHD vapor before and after exposure to the 253.7 nm UV light of a low-pressure mercury vapor lamp are presented in

dx.doi.org/10.1021/jp201110p |J. Phys. Chem. A 2011, 115, 7494–7502

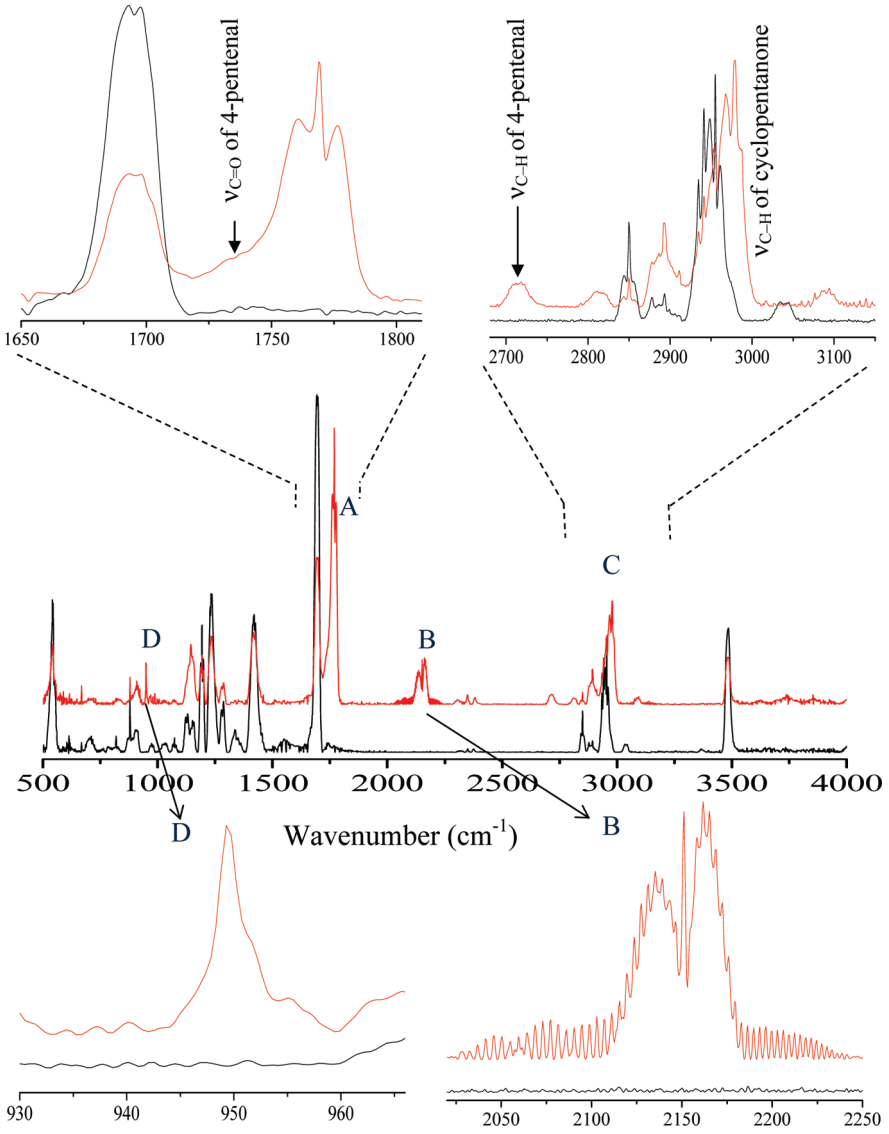

Figure 5. Infrared spectra of α-CHD vapor before (black trace) and after UV exposure (red trace). Four small segments of the two spectra, denoted by A, B, C and D, are shown in expanded frequency scales.

Figure 4 (panels A and B). The base peak in the mass spectrum of panel A (before UV exposure) is the intact molecular ion, and the peaks corresponding to m/z values of 84 and 70 are assigned to cation fragments produced following loss of CO/C_2H_4 (28) and ketene (42), respectively from the parent molecular ion. Tentatively, we also suggest that the species correspond to m/z = 84 and 70 are cyclopentanone and ethyl ketene cations, respectively. We show below using infrared spectral results that the peak at 83 is likely to be arising by loss of H atom from the molecular ion of 4-pentenal, an isomeric aldehyde of cyclopentanone. The peak for m/z = 56 has been corresponded to the molecular ion of methyl ketene.

Panel B shows that the intensities of all peaks, except the one for m/z = 70, are enhanced with respect to the parent ion peak upon photolysis. This implies that no photoproduct of mass 70 is produced. The new peaks for m/z = 28 in the mass spectrum B could be due to CO^+ or $C_2H_4^+$ ions. However, the ionization energy of CO being larger compared to the kinetic energy of the electrons used for ionization of the sample molecule, the peak at the mass channel 28 has been corresponded to ethylene cation only. The infrared spectral features (see Figure 5) of the photoproducts indicate that CO is also produced in quite abundant extent. The peak for m/z = 42 has been assigned to ketene (CH_2CO^+) ion. The enhanced intensity of the peak for m/z = 84 implies that cyclopentanone is produced following decarbonylation of the electronically excited α-CHD molecules, and this has been verified by infrared spectroscopy. The electron ionization mass spectrum of cyclopentanone measured under the same condition (ionization electron KE = 11 eV) is presented in panel C. It is seen that the parent molecular ion is the base peak in spectrum and two fragment ions appear at m/z = 55 and 56. Therefore, a comparison of this spectrum with that of panel B indicates the origin of enhanced intensity for 84 and 56 is due to ionization/fragmention of the photoproduct. There is a substantial increase in intensity of the ion peak of mass 55, and this can be corresponded to $CH_2{=}CH{-}C{\equiv}O^+$ ion.

4.2. Gas Phase FTIR Spectroscopy. The mid-IR spectra of α-CHD vapor, measured before (bottom panel, black) and after

dx.doi.org/10.1021/jp201110p |J. Phys. Chem. A 2011, 115, 7494–7502

Scheme 1. Primary Photoreaction Channels of α-CHD Proposed on the Basis of the Identified Photoproducts

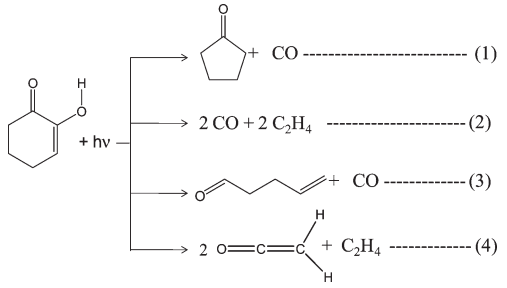

Scheme 2. Primary Photoreaction Channels of Cyclopentatone Proposed in Ref 39−42

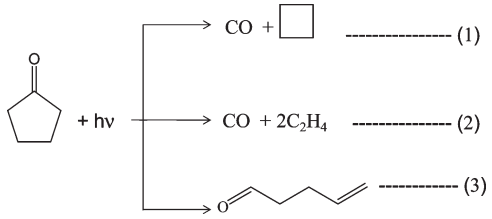

UV exposure (top panel, red) are presented in Figure 5. The vibrational features for the photophotoproducts appear only in four segments of the latter spectrum labeled A, B, C, and D, and we explain below that the product molecules responsible for these bands are carbon monoxide, cyclopentanone, ethylene, ketene, and 4-pentenal. In segment A (blown up at top left), the double-headed band near 1700 cm^{-1} in the spectrum of the pre-exposed (UV) sample vapor is the $\nu_{C=O}$ band of the monoenol tautomer of α-CHD. The band developed in the spectrum near 1775 cm^{-1} upon UV exposure that has characteristic rotational contour corresponding to P, Q, and R branches is the $\nu_{C=O}$ transition of the photoproduct cyclopentanone, and this has been verified by recording the FTIR spectrum of pure cyclopentanone vapor. The feature that weakly develops at ∼1730 cm^{-1} has been assigned to $\nu_{C=O}$ of 4-pentenal, an isomer of cyclopentanone. The characteristic $\nu_{C—H}$ of this aldehyde appears at 2720 cm^{-1}, as shown in the expanded view of the segment C. The other characteristic feature of this compound, the ethylenic ═C—H stretches, appears weakly at 3090 cm^{-1}. This aldehyde and cyclopentanone together is responsible for the mass peak at 84, and the weak feature at 83 could arise following H atom loss from the 4-pentenal cation.

In the fingerprint region, the band labeled D at 950 cm^{-1} is the characteristic feature of ethylene and it represents a fundamental corresponding to wagging mode (b_{1u} symmetric) of the two CH_2 groups of the molecule, and this assignment is also consistent with appearance of the mass peak at 28. The C−H stretching fundamentals ($\nu_{C—H}$) of ethylene superpose on the same of 4-pentenal and appear as broad feature near 3090 cm^{-1} (segment C), and the same transitions for cyclopentanone appear more prominent in the same region of the spectrum. In segment B, a vibrational band with prominent P, Q, and R branches appears at 2150 cm^{-1} (the position for the sharp Q-branch). This band is built over the background of long P−R branches of the vibration−rotational transitions of the $\nu_{C=O}$ transition of carbon monoxide. The former has been assigned to $\nu_{C=O}$ of ketene and it is consistent with the mass peak at 42 in Figure 4, panel B.

5. PHOTOLYSIS MECHANISMS

On the basis of the analysis of photoproducts presented above, we propose the reaction channels in Scheme 1, via which the reactions can take place upon electronic excitation of α-CHD by the UV light of wavelength 253.7 nm in the gas phase.

The relative intensities of the key features of the product molecules in both the mass and IR spectra reveal that the reaction channel 1 is preferred most, which resembles with the most preferred dissociation channel of the cyclic monoketones of comparable ring size, e.g., cyclopentanone and cyclohexanone. According to refs 39−42, the major photodecomposition channels of cyclopentanone are as given in Scheme 2.

Here an interesting feature of the reactions is that channel 1 is dominant for both α-CHD and cyclopentanone, in spite of the fact that the nature of the excited states produced are different when the two molecules are excited by light of common wavelength, λ = 253.7 nm. As explained before, the monoketones are excited to the lowest $n\pi^*$ state (S_1), whereas, α-CHD is likely to be excited to S_2, which has been predicted to be significantly $\pi\pi^*$ in nature.

A pertinent question concerning the reaction mechanism is the electronic state at which the primary step, α-cleavage, takes place. In the case of α-CHD, of the three possible sites for α-cleavage, the rupture of $C_1—C_2$ bond appears to be essential to explain formation of all the photoproducts (presented below). The α-cleavage in cyclic monoketones can take place at either the lowest triplet (T_1) or higher vibrational levels of the ground (S_0) state, or both. An exception is the case of cyclobutanone, where this step can occur in S_1 by means of a predissociation mechanism.[13] In Figure 3 we have presented the optimized geometries in three electronic states (S_0, S_1, and S_2) of α-CHD, and it indicates that no bond is significantly weakened upon electronic excitation. Furthermore, we present below additional discussion to justify that $C_1—C_2$ bond cleavage can also not occur at the Franck−Condon level in S_2 upon absorption of the 253.7 nm wavelength photon. However, similar to the case of monoketones, the said bond breaking can occur in the T_1 surface and also at the higher vibrational levels of S_0. Both T_1 and higher vibrational levels of S_0 of α-CHD can be populated via intersystem crossing and internal conversion processes, respectively. In general, the carbonyl compounds are known to undergo efficient $T_1 \leftarrow S_1$ intersystem crossing upon $n\pi^*$ (S_1) excitation, and this was probed by measuring phosphorescence ($S_0 \leftarrow T_1$ transition) as well as transient absorption spectra (T_1 to higher triplet states).[10]

In Figure 6 we have presented potential energy (PE) curves as a function of $C_1—C_2$ bond length for the ground (S_0) and five lowest excited electronic states (S_1, S_2, T_1, T_2, and T_3) calculated by use of DFT/B3LYP/6-311++G** and TDDFT/B3LYP/6-311++G** theoretical methods, respectively. The molecular geometries in the ground state for discrete values of $C_1—C_2$ were optimized partially, and the energies with respect to that of the fully optimized configuration are plotted to generate the PE curve for S_0 state. For excited states, the curves were generated by plotting the calculated vertical transition energies corresponding to different partially optimized geometries. These PE curves

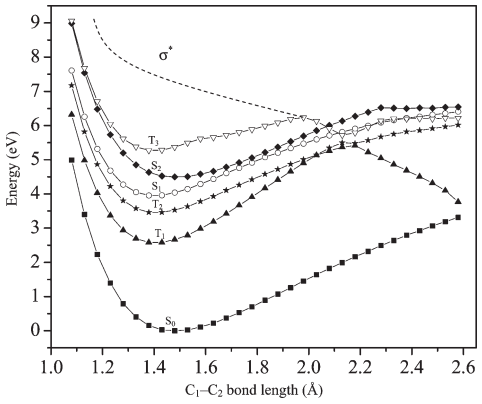

Figure 6. Potential energy curves for the lowest five electronic states of α-CHD as a function of C_1-C_2 bond length. The curve for T_1 is predicted dissociative for values of C_1-C_2 > ~2.15 Å and it involves transition to a σ^* orbital corresponding to this bond. At equilibrium geometry, the transition is expected to be occurring at a very high energy, denoted by dashed line.

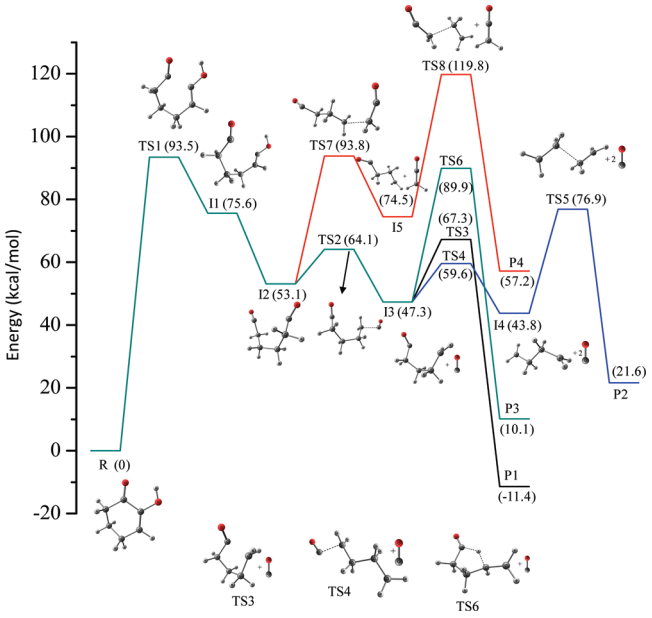

Figure 7. Various transition states and intermediates for thermal dissociation of α-CHD (R) according to reaction channels 1−4 shown in Scheme 1. The energies of various intermediates (Ix) and products (Px) depicted on the ground global potential energy surface of α-CHD are relative to the energy of the optimized geometry of monoenol tautomer of the molecule. Px corresponds to the reaction channel x in Scheme 1.

indicate that the molecule cannot undergo dissociation from the low-lying vibrational levels of any of the five excited electronic states, and they are bound in equilibrium configurations. The possibility for direct dissociation of the C_1-C_2 bond at the Franck−Condon level is ruled out on the basis of the following arguments. The spectrum presented in Figure 1 indicates that the excess vibrational energy acquired in S_2 electronic state upon absorption at 253.7 nm cannot be larger than ~0.5 eV. In contrast, the approximate potential energy curve for S_2 indicates that the required vibrational energy to reach at the dissociation threshold for the C_1-C_2 bond could be much larger. Of course, for more accurate prediction one needs to take into account of the zero-point energy. Therefore, the possibility for direct dissociation of the molecule at this surface is likely to be infeasible.

On the other hand, the nature of the T_1 potential energy curve indicates that this electronic state shows dissociative character for C_1-C_2 bond length longer than 2.15 Å. It implies that if T_1 is prepared with high vibrational energy, particularly with respect to the C_1-C_2 stretching mode, α-cleavage can take place in this electronic state. The transition from initially prepared levels to these levels can occur by means of intersystem crossing mechanism. Visualization of the molecular orbitals in such situation reveals that T_1 corresponds to excitation of the molecule to the σ^* orbital of the C_1-C_2 bond, whereas, at the equilibrium geometry, T_1 corresponds with the lowest $n\pi^*$ state. This clearly indicates that dissociative nature of the PE curve of T_1 for C_1-C_2 >2.15 Å occurs for crossing of the $\sigma^*(C_1-C_2)$ orbital with the lowest π^* orbital. Energetically, the crossing occur nearly 3 eV above the energy minimum of the T_1 curve. The effect of crossing of this σ^* orbital with the π^* orbital corresponding to T_1 and T_3 states are manifested in the potential energy curves for C_1-C_2 values in the range of 1.95−2.15 Å. For C_1-C_2 < 1.9 Å, the potential energy curve of σ^* state as a function of C_1-C_2 bond length is qualitatively shown using dashed line, and a direct excitation to this level from S_0 is likely to be occurring only with very high excitation energy. From the energetic viewpoints, the most obvious possibility for occurrence of bond cleavage is at the higher vibrational levels of S_0, which can be produced by both internal conversions from S_2 or via intersystem crossing mechanisms from the low lying triplet states.

In Figure 7 we have shown a few probable steps through which the reactions shown in Scheme 1 could take place in the ground electronic state (thermal reaction) to generate the five identified final products. The relative energies of various intermediates and transition states along the said reaction channels are shown. The geometry optimizations corresponding to these configurations have been performed at RHF/6-311++G** and DFT/RB3LYP/6-311++G** levels for molecules with closed shell electronic configurations, and at UHF/6-311++G** and DFT/UB3LYP/6-311++G** levels for open shell radicals. Here we have shown only the predictions of RHF and UHF calculations, and those of B3LYP and UB3LYP calculations are presented as Supporting Information. It has been found that the basic energetic features predicted by the calculations at the two said levels of theory (HF and B3LYP) are not different, and in some cases the specific energies are same. For example, the barrier for α-cleavage, the first step of the reaction, is predicted almost same by the two calculations. Second, relative preferences for different product formation channels are also predicted the same. These predictions are valuable to understand the relative yields for various reaction products. The transition state configurations for all reaction steps are verified by performing IRC calculation. The cyclopentanone formation is predicted exothermic, whereas the other reactions are endothermic. Consequently, the former channel is expected to be preferred over the other reactions, and this is consistent with observations. In Figure 4 (panel B) the combined intensity for m/z = 84 (cyclopentanone cation) and 55/56 (ionic fragments produced via dissociation of cyclopentanone cation) is much larger compared to that for m/z = 42 (ketene ion). Likewise, in the infrared spectrum (Figure 5) the $\nu_{C=O}$ of cyclopentanone appears more intense compared to that of ketene.

The predicted activation energy barrier to rupture the C_1-C_2 bond of the enol tautomer of α-CHD (R) in the ground electronic state is ∼94 kcal/mol (TS1). This energy being many times larger compared to thermal energy, the reaction cannot occur unless the molecules are prepared to highly vibrationally excited states to meet the energy requirement for crossing the activation barrier. Such high vibrational excitations can be realized via internal conversions of the excited electronic state produced by light absorption. The keto−enol form of the diradical (I1) generated immediately after ring-opening is likely to be converted to more stable diketo form (I2), because, the former can no longer be stabilized by any intramolecular hydrogen bonding like its precursor, and the latter is more stable by ∼23 kcal/mol (HF/6-311++G**). For the reactions to occur via channels 1, 2, and 3, the next common step is decarbonylation of I2 resulting in formation of the intermediate I3. For this step, there is a small energy barrier (TS2) with respect to the optimized conformation of I2. Subsequently, for formation of cyclopentanone (channel 1) and further ruptures of two C−C bonds (channel 2) there are a few activation barriers to cross, e.g., TS3, TS4, and TS5. However, the magnitude of these barriers being smaller compared to TS1, the internal energy content of the generated diradical (I2) is expected to be sufficient to cross the subsequent barriers without acquiring additional energy. Reaction channel 3 involves a prototropic isomerization of the intermediate I3. Although the barrier for this step (TS6) with respect to the optimized geometry of I3 is predicted 43 kcal/mol, and it is higher compared to the barriers for other two channels (TS3 and TS4), the former reaction can occur via tunneling mechanism as it involves displacement of a hydrogen atom. For reaction channel 4, calculation suggests an intermediate I5 following release of the first ketene molecule. Although the release of second ketene molecule from I5 is not favorable energetically, it can decay via other favored pathways. For example, a radical recombination of two I5 species is highly exothermic ($2O{=}\dot{C}{-}CH_2{-}CH_2{-}\dot{C}H_2 \rightarrow O{=}\dot{C}{-}(CH_2)_6{-}\dot{C}{=}O$, $\Delta E \sim -60$ kcal/mol), and the dimeric adduct can dissociate into CO, C_2H_4, and cyclopentanone via energetically much favored pathways.

6. SUMMARY

In this paper we have presented the UV photolysis of α-CHD vapor carried out by exciting with the 253.7 nm line of a mercury vapor lamp. Theoretical calculation at TDDFT/B3LYP/6-311++G** level predicts that the excited state produced upon absorption at this wavelength has a significant extent of $\pi\pi^*$ character. The absorption cross-section of the molecule at this wavelength is about 3 orders of magnitude larger than those of the analogous linear diketones and also of monoketones. Product analysis using a combination of mass spectrometry and infrared spectroscopy reveals that decarbonylation along with cyclopentanone formation is the major reaction channel. Three other reaction channels that we have proposed give rise to formation of ketene, ethylene, and 4-pentenal. The potential energy curves as a function of C−C bond length between two carbonyl groups (C_1-C_2), calculated at the same level of theory, suggest that the molecule is bound in the equilibrium configurations of the ground (S_0) and five low-lying excited electronic states (S_1, S_2, T_1, T_2, and T_3). In fact, the C_1-C_2 bond gains partial double bond character in all the excited states. However, for $C_1-C_2 >$ 2.15 Å, the potential energy curve in T_1 state appears repulsive. A scrutiny of the molecular orbitals reveals that this happens because of crossing of the lowest $n\pi^*$ state with an $n\sigma^*$ state beyond the said C_1-C_2 bond distance. Thus, we propose that the primary photolysis step, ring rupture (α-cleavage) leading to formation of the diradical, can occur in the lowest triplet (T_1) state. The said α-cleavage can also take place in the ground electronic state and the activation barrier calculated for this is ∼94 kcal/mol. This energy being smaller than the energy quantum of 253.7 nm light, the higher vibrational levels in S_0 can be prepared by internal conversion mechanism following electronic absorption. According to our calculation, cyclopentanone formation in the ground state is exothermic but other channels that generate ketene, ethylene, and 4-pentenal are endothermic. These predictions are consistent with the observed yields of the photolysis products.

■ ASSOCIATED CONTENT

Supporting Information. Activation energy barriers and energies for different intermediates and final products for the thermal reaction at ground electronic state surface using DFT/B3LYP/6-311++G** level. This information is available free of charge via the Internet at http://pubs.acs.org.

■ AUTHOR INFORMATION

Corresponding Author
*E-mail: pctc@iacs.res.in.

■ ACKNOWLEDGMENT

We sincerely thank the Department of Science and Technology, Government of India, for financial support to carry out the research presented here. Technical assistance extended by Nishith, Jhankar, and Prabir to build the apparatus are also acknowledged.

■ REFERENCES

(1) Klessinger, M.; Michl, J. *Excited States and Photochemistry of Organic Molecules*; VCH: New York, NY, 1995.
(2) Nádasdi, R.; Zügner, G. L.; Farkas, M.; Dóbé, S.; Maeda, S.; Morokuma, K. *Chem. Phys. Chem.* **2010**, *11*, 3883.
(3) Maeda, S.; Ohno, K.; Morokuma, K. *J. Phys. Chem. Lett.* **2010**, *1*, 184.
(4) Zhu, C.; Zhu, L. *J. Phys. Chem. A* **2010**, *114*, 8384.
(5) Zhang, P.; Maeda, S.; Morokuma, K.; Braams, B. J. *J. Chem. Phys.* **2009**, *130*, 114304.
(6) Araujo, M.; Lasorne, B.; Bearpark, M. J.; Robb, M. A. *J. Phys. Chem. A* **2008**, *112*, 7489 and references therein.
(7) Rajakumar, B.; Gierczak, T.; Flad, J. E.; Ravishankara, A. R.; Burkholder, J. B. *J. Photochem. Photobiol. A: Chem.* **2008**, *199*, 336.
(8) Wang, Q.; Wu, D.; Jin, M.; Liu, F.; Hu, F.; Cheng, X.; Liu, H.; Hu, Z.; Ding, D.; Mineo, H.; Dyakov, Y. A.; Mebel, A. M.; Chao, S. D.; Lin, S. H. *J. Chem. Phys.* **2008**, *129*, 204302.
(9) Badr, Y.; Mahmoud, M. A. *J. Mol. Struct.* **2005**, *748*, 189.
(10) Haas, Y. *Photochem. Photobiol. Sci.* **2004**, *3*, 6 and references therein.
(11) Diau, E. W.; Kötting, G. C.; Sølling, T. I.; Zewail, A. H. *Chem. Phys. Chem.* **2002**, *3*, 57 and references therein.
(12) Diau, E. W.; Kötting, G. C.; Zewail, A. H. *Chem. Phys. Chem.* **2001**, *2*, 273.
(13) Diau, E. W.; Kötting, G. C.; Zewail, A. H. *Chem. Phys. Chem.* **2001**, *2*, 294.
(14) Kosmidis, C.; Philis, J. G.; Tzallas, P. *Phys. Chem. Chem. Phys.* **1999**, *1*, 2945.

(15) Fahr, A.; Braun, W.; Laufer, A. H. *J. Phys. Chem.* **1993**, *97*, 1502.
(16) Moortgat, G. K.; Meyrahn, H.; Warneck, P. *Chem. Phys. Chem.* **2010**, *11*, 3896.
(17) Iwasaki, E.; Matsumi, Y.; Takahashi, K.; Wallington, T. J.; Hurley, M. D.; Orlando, J. J.; Kaiser, E. W.; Calvert, J. G. *Int. J. Chem. Kinet.* **2008**, *40*, 223.
(18) Kusaba, M.; Tsunawaki, Y. *Radiat. Phys. Chem.* **2007**, *76*, 1447.
(19) Smith, G. D.; Molina, L. T.; Molina, M. J. *J. Phys. Chem. A* **2002**, *106*, 1233.
(20) Emrich, M.; Warneck, P. *J. Phys. Chem. A* **2000**, *104*, 9436.
(21) Aloisio, S.; Francisco, J. S. *Chem. Phys. Lett.* **2000**, *329*, 179.
(22) Klotz, B.; Graedler, F.; Sørensen, S.; Branes, I.; Becker, K. *Int. J. Chem. Kinet.* **2001**, *33*, 9.
(23) Gierczak, T.; Burkholder, J. B.; Bauerle, S.; Ravishankara, A. R. *Chem. Phys.* **1998**, *231*, 229.
(24) Koch, S.; Moortgat, G. K. *J. Phys. Chem. A* **1998**, *102*, 9142.
(25) Gierczak, T.; Burkholder, J. B.; Talukdar, R. K.; Mellouki, A.; Barone, S. B.; Ravishankara, A. R. *J. Photochem. Photobiol A: Chem.* **1997**, *110*, 1.
(26) Sakurai, H.; Kato, S. *J. Mol. Struct (THEOCHEM)* **1999**, *461*, 145.
(27) Horowitz, A.; Meller, R.; Moortgat, G. K. *J. Photochem. Photobiol. A: Chem* **2001**, *146*, 19.
(28) Jackson, A. W.; Yarwood, A. J. *Can. J. Chem.* **1972**, *50*, 1338.
(29) Samanta, A. K.; Pandey, P.; Bandyopadhyay, B.; Chakraborty, T. *J. Mol. Struct.* **2010**, *963*, 234.
(30) Bell, W. E.; Blacet, F. E. *J. Am. Chem. Soc.* **1954**, *76*, 5332.
(31) Kupchan, S. M.; Britton, R. W.; Lacadie, J. A.; Ziegler, M. F.; Sigel, C. W. *J. Org. Chem.* **1975**, *40*, 648.
(32) Fukamiya, N.; Lee, K.; Muhammad, I.; Murakami, C.; Okano, M.; Harvey, I.; Pelletier, J. *Cancer Lett.* **2005**, *220*, 37.
(33) (a) Hoffken, K.; Jonat, W.; Possinger, K.; Kolbel, M.; Kunz, T. H.; Wagner, H.; Becher, R.; Callies, R.; Friederich, P.; Willmanns, W.; Maass, H.; Schmidt, C. G. *J. Clin. Oncol.* **1990**, *8*, 875. (b) Pickles, T.; Perry, L.; Murray, P.; Plowman, P. *Br. J. Cancer* **1990**, *62*, 309.
(34) Gianturco, M. A.; Giammarino, A. S.; Pitcher, R. G. *Tetrahedron* **1963**, *19*, 2051.
(35) Francis, J. T.; Hitchcock, A. P. *J. Phys. Chem.* **1994**, *98*, 3650.
(36) Bouchoux, G.; Hoppilliard, Y.; Houriet, R. *New. J. Chem.* **1987**, *11*, 225.
(37) Shen, Q.; Traetteberg, M.; Samdal, S. *J. Mol. Struct.* **2009**, *923*, 94.
(38) Frisch, M. J.; et al. *Gaussian 03*, revision E.01; Gaussian, Inc.: Wallingford, CT, 2004.
(39) Mok, C. Y. *J. Phys. Chem.* **1970**, *74*, 1432.
(40) Srinivasan, R. *J. Am. Chem. Soc.* **1961**, *83*, 4344.
(41) Blacet, F. E.; Millerc, A. *J. Am. Chem. Soc.* **1957**, *79*, 4327.
(42) Shortridge, R. G., Jr.; Lee, E. K. C. *J. Phys. Chem.* **1973**, *77*, 1936.